# Impact of Moisture Flux and Freezing Level on Simulated Orographic Precipitation Errors over the Pacific Northwest

YANLUAN LIN

*Ministry of Education Key Laboratory for Earth System Modeling, Center of Earth System Sciences, Tsinghua University, Beijing, China*

BRIAN A. COLLE

*School of Marine and Atmospheric Sciences, Stony Brook University, Stony Brook, New York*

SANDRA E. YUTER

*Department of Marine, Earth, and Atmospheric Sciences, North Carolina State University, Raleigh, North Carolina*

(Manuscript received 26 January 2012, in final form 20 September 2012)

ABSTRACT

Two cool seasons (November–March) of daily simulations using the fifth-generation Pennsylvania State University–NCAR Mesoscale Model (MM5) over the Pacific Northwest are used to investigate orographic precipitation bias. Model simulations are compared with data from a radiosonde site at Salem, Oregon, just upstream (west) of the Oregon Cascades; precipitation gauges over a portion of the Pacific Northwest; and a National Weather Service Weather Surveillance Radar-1988 Doppler (WSR-88D) in Portland, Oregon. The 77 storms analyzed are partitioned into warm/cold storms based on the freezing level above/below the Oregon Cascades crest (~1600 m MSL). Although the seasonal precipitation is well simulated, the model has a tendency to overpredict surface precipitation for cold storms. The correlation between the upstream relative humidity–weighted integrated moisture transport and precipitation for warm storms ($r^2 = 0.81$) is higher than that for cold storms ($r^2 = 0.54$). Comparisons of model ice water content (IWC) and derived reflectivity with radar-retrieved IWC and observed reflectivity for the 38 well-simulated storms show reasonably good agreement for warm storms but an overprediction of IWC and reflectivity aloft for cold storms. One plausible reason for the persistent overprediction of IWC in cold storms might be related to the positive bias in snow depositional growth formulation in the model bulk microphysics parameterization. A favorable overlap of the maximum snow depositional growth region with the mountain wave ascent region in cold storms magnifies the bias and likely contributes to the precipitation overprediction. This study also highlights the benefit of using data aloft from an operational radar to complement surface precipitation gauges for model precipitation evaluation over mountainous terrain.

## 1. Introduction

Quantitative precipitation forecasting (QPF) continues to be a significant challenge (Ralph et al. 2005). Winter precipitation over the Pacific Northwest is usually related to a combination of synoptic-scale storms from the Pacific Ocean and terrain forcing (e.g., Neiman et al. 2011; Yuter et al. 2011). Several studies have investigated the impacts of horizontal resolution and different microphysical parameterizations on simulated orographic precipitation (e.g., Colle et al. 1999; Colle and Mass 2000; Leung and Qian 2003; Grubišić et al. 2005; Mass et al. 2002; Garvert et al. 2005a,b; Lin and Colle 2009). At relatively high resolution (1–2-km grid spacing), the horizontal flow, vertical motion, and precipitation distributions are realistically represented over terrain (Garvert et al. 2005b; Colle et al. 2005); however, numerous precipitation biases over terrain at high resolution have been noted. These biases have been attributed in part to deficiencies in the model bulk microphysical

*Corresponding author address:* Dr. Yanluan Lin, Ministry of Education Key Laboratory for Earth System Modeling, Center of Earth System Sciences, Tsinghua University, Beijing 100084, China.
E-mail: yanluan@mail.tsinghua.edu.cn

DOI: 10.1175/JHM-D-12-019.1

parameterizations (BMPs) (e.g., Colle and Mass 2000; Garvert et al. 2005b; Milbrandt et al. 2008, 2010). In addition to the model BMPs, errors from synoptic and mesoscale kinematic and thermodynamic fields also impact model QPF (Richard et al. 2007; Roebber et al. 2008; Minder et al. 2008; Schlemmer et al. 2010).

Low-level moisture flux is an important ingredient for orographic precipitation (Smith 1979). The strong correlation between upstream water vapor transport and orographic precipitation has been documented in many locations, such as along the California coast (Neiman et al. 2002; Smith et al. 2010), the European Alps (Smith et al. 2003; James et al. 2004; Muller and Kaspar 2011), and the Andes (Smith and Evans 2007; Falvey and Garreaud 2007). Colle et al. (2008) and Hahn and Mass (2009) used a case study approach to show that the accuracy of the predicted precipitation over the Pacific Northwest is dependent on the upstream moisture flux errors. The drying ratio (DR) (Smith et al. 2005) is a metric of the relative amount of water vapor removed by precipitation compared to the inflow water vapor. It follows that the larger the observed drying ratio, the stronger the dependence of model precipitation errors on upstream moisture flux errors. Smith et al. (2005) estimated an annual drying ratio of 0.43 for Oregon.

Operational radar observes precipitation-sized particles in a three-dimensional volume and thus provides a way to complement surface precipitation evaluation. Surface precipitation is essentially the accumulation of vertical mass flux of precipitating hydrometeors. Thus, precipitating hydrometeors aloft is closely related to surface precipitation by the fall speeds of hydrometeors. Ground-based radars have been used to evaluate the model precipitation and wind structures over a barrier for specific case studies, but operational radars have not been used previously over multiple seasons to evaluate the model precipitation predictions over mountainous terrain.

Analysis of a large sample of storms from two cool seasons allows us to take previous work a step further. Large samples of storms help identify systematic biases. In this paper, we examine how variations in freezing-level height can modify both the observed relationship between inflow moisture flux and precipitation as well as the relationship between model errors in moisture flux and errors in predicted precipitation. We utilize gauge, radiosonde, and three-dimensional radar datasets to deduce potential sources of surface precipitation error within the model. Combining upstream moisture flux, precipitating hydrometeors aloft, and surface precipitation together gives a complement framework for model precipitation evaluation. This also helps identify model potential error sources.

After describing the experiment setup and observational datasets in section 2, the model precipitation performance and its connection to upstream moisture flux and freezing-level height are presented in section 3. Section 4 summarizes the main results with a brief discussion.

## 2. Model setup and observational datasets

### *a. Model setup*

The fifth-generation Pennsylvania State University–National Center for Atmospheric Research Mesoscale Model (MM5) version 3.7 was used with 1.33-, 4-, and 12-km domains nested within a 36-km domain covering a wide region of the eastern Pacific and Pacific Northwest (not shown). The 4-km domain covers a portion of Washington and Oregon (Fig. 1), while the 1.33-km domain is centered over parts of southwestern Washington and northwestern Oregon. The MM5 was used in this study rather than the Weather Research and Forecasting Model (WRF; Skamarock et al. 2008) since 1) many orographic precipitation case studies in this region have used MM5 (e.g., Colle and Mass 2000; Grubisić et al. 2005; Mass et al. 2002; Garvert et al. 2005a,b) and 2) this study is not to verify the latest model and parameterizations, but rather to generalize some of the previous case study results and to illustrate the influences of moisture flux and freezing level on the precipitation errors, which can occur for any modeling system. The Thompson et al. (2004) BMP in MM5 was replaced with the Thompson et al. (2008) version, which was available in version 2 of WRF, so that these results can be related to other WRF studies using this scheme (Thompson et al. 2008; Colle et al. 2008; Lin and Colle 2009).

For the 2005/06 and 2006/07 cool seasons (November–March), the MM5 was run twice daily to 24 h starting at 0000 and 1200 UTC, with initial and lateral boundary conditions derived from the 6-h National Centers for Environmental Prediction (NCEP) Global Forecast System (GFS) model analyses at 1° spacing. The snow cover for each MM5 run was initialized using the Rapid Update Cycle (RUC) analysis (20-km horizontal spacing), whereas the sea surface temperature, soil temperature, and soil moisture were obtained from the GFS analysis. The 4- and 1.33-km domains were initialized at 0600 and 1800 UTC using the 6-h forecast from the 12-km domain using a one-way nesting. Four-dimensional data assimilation (analysis nudging; Stauffer and Seaman 1990) was used during the first 12 h of the 36- and 12-km domains. The goal of nudging the outer domains and the use of GFS analysis boundary conditions was to reduce the large-scale errors in order to investigate the

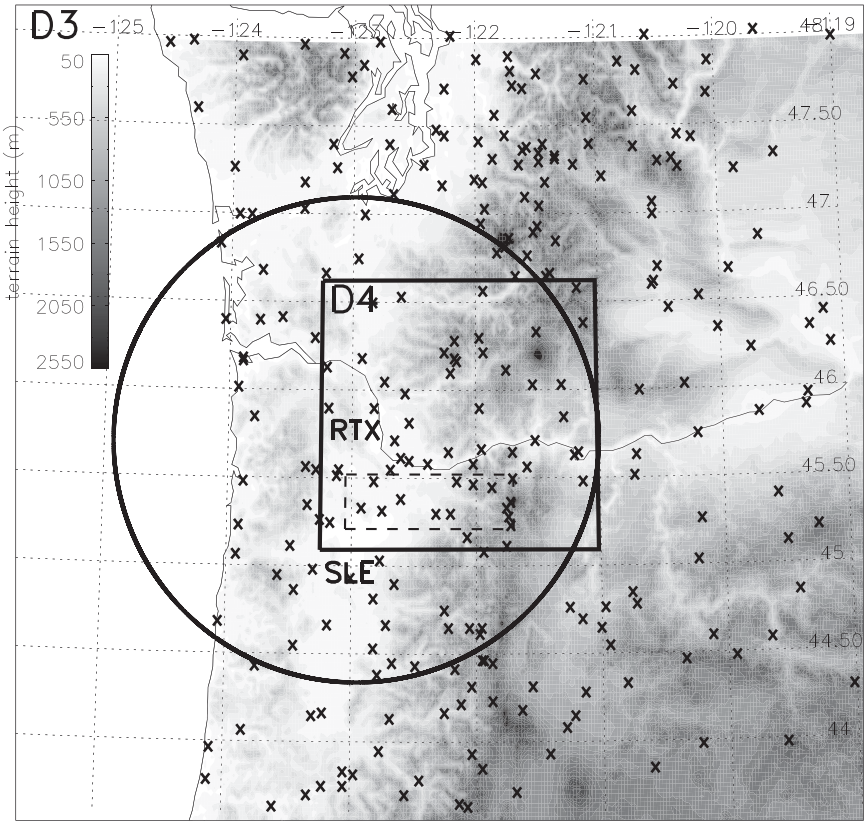


FIG. 1. Model 4- and 1.33-km domain with observational facilities overlaid. The black circle indicates the 150-km range of the WSR-88D at Portland (RTX); crosses are the precipitation gauge sites. SLE is the radiosonde site at Salem, OR. The dashed west–east box is the cross section used in Fig. 6.

short-term performance within the inner nests. The last 12 h of the 18-h simulation (6–18 h) from the 4- and 1.33-km domains were used for verification.

The model physics include the eta planetary boundary layer (PBL) (Janjić 1994), Thompson microphysics (Thompson et al. 2008), Dudhia (1989) short- and longwave radiative transfer, and MM5 simple slab land surface model. The modified Kain–Fritsch cumulus scheme (Kain and Fritsch 1993; Kain 2004) was used in the 36- and 12-km domains. A positive definite moisture advection (PDA) scheme (Skamarock 2006) was not available in MM5. Hahn and Mass (2009) showed a PDA moisture scheme in WRF can reduce the surface precipitation by 3%–17% over the Pacific Northwest for a particular case study. Lin and Colle (2009) noted an approximately 10% reduction of surface precipitation when using PDA for another case study over the Oregon Cascades. The interpretation of the precipitation verification results in this study includes an expectation of model surface precipitation overprediction of up to 20%, since PDA was not used.

### b. Observational datasets

#### 1) PRECIPITATION GAUGE NETWORK

Daily liquid-equivalent precipitation data from the National Weather Service (NWS) Cooperative Observer Program (COOP) stations and the National Resources Conservation Services (NRCS) snowpack telemetry (SNOTEL) sites (Fig. 1) were synthesized to evaluate the model surface precipitation performance. Previous studies by Garvert et al. (2005b) and Colle et al. (2008) have suggested that 1.33-km grid spacing better resolves the vertical motions over the Cascade Mountains than 4-km grid spacing; thus, the precipitation verification in this paper will focus on the 1.33-km domain. The twice-daily precipitation forecasts (6–18 h) from the 1.33-km MM5 domain were interpolated to the gauge locations using an inverse distance (Cressman 1959) approach, as in Colle et al. (1999), and summed to get the model 24-h precipitation. We define model precipitation bias score for a storm as the ratio between the mean forecast precipitation for all stations

(56 in total) within the 1.33-km domain and the observed mean precipitation at these same stations. The inhomogeneous spatial distribution of these gauge stations may introduce some representative uncertainties. Precipitation gauge undercatchment is difficult to quantify and depends on precipitation types and snowflake types (Groisman and Legates 1994; Colle and Mass 2000; Theriault et al. 2012). Groisman and Legates (1994) estimated a roughly 5%–15% gauge undercatchment error for rain. The accuracy of snow measurement depends on both the wind speed and the type of snowflake, and undercatchment for snow can be up to 50% under windy conditions (Theriault et al. 2012). This might explain some of the different biases for warm and cold storms discussed later. To account for some precipitation gauge undercatchment (~10%) and not using PDA for moist variables (20%), the over- and underprediction days in the analysis are defined as bias scores greater than 1.3 and less than 1.0, respectively.

#### 2) RADIOSONDE

Radiosonde observations of wind, pressure, temperature, and moisture are made twice daily (0000 and 1200 UTC) at Salem, Oregon (SLE in Fig. 1). Both the 4-km MM5 and observed meteorological variables were linearly interpolated to a vertical grid spacing of 200 m between 100 and 7900 m MSL. To relate the 12-hourly SLE soundings to the daily precipitation, daily profiles of moisture, winds, and temperature were computed following Falvey and Garreaud (2007):

$$X = (X_{-12h} + 2X_0 + X_{12h})/4, \quad (1)$$

where $X_{-12h}$ and $X_{12h}$ are moisture, winds, and temperature observations 12 h before and 12 h after the radiosonde observations at 1200 UTC $X_0$.

A dry bias has been noted for the Vaisala radiosonde (e.g., Turner et al. 2003), and we found a similar dry bias during saturated conditions in the SLE sounding (not shown). Therefore, following Turner et al. (2003), we apply a 5% increase of relative humidity (RH) to the SLE sounding, with the caveat that RH cannot exceed 100% with respect to water. The 4-km MM5 forecasts every 12 h at forecast hour 6 (0000 and 1200 UTC) were interpolated to the Salem site, and the same daily average method given in Eq. (1) was used to get the model daily sounding. The model and observed column-integrated RH-weighted moisture flux (for simplicity, called moisture flux hereafter) was computed from the sounding. Wind and temperature near the crest level (1.5 km MSL) are used for later storm categorization.

#### 3) WSR-88D

The NWS Weather Surveillance Radar-1988 Doppler (WSR-88D) at Portland, Oregon (RTX in Fig. 1), provided information of the three-dimensional precipitation structures within the 150-km range of the radar. The Level II data were interpolated to a grid with 2-km spacing in the horizontal and 1-km spacing in the vertical at about 6-min time intervals following Yuter et al. (2011). The 1.33-km MM5 outputs at 15-min intervals are interpolated horizontally and vertically to the corresponding radar grid points.

To compare the model cloud and precipitation with radar directly, both model-derived radar reflectivity and radar-retrieved ice water content (IWC) above the freezing level are used. Model reflectivity is calculated in the Rayleigh scattering regime using the microphysical assumptions in Thompson et al. (2008), including particle size distribution and mass–dimension relationship. IWC retrieval from centimeter-band radar has not been extensively explored and can have substantial uncertainties due to the ice particle shapes, size distribution, and mass–dimension relationship, among others (e.g., Protat et al. 2007; Heymsfield et al. 2008). We follow Hogan et al. [2006, their Eq. (14)] to retrieve IWC using radar reflectivity and temperature. As in Hogan et al. (2006), only measurements with an observed column maximum reflectivity larger than 12 dB$Z$ are used, which includes primarily precipitation conditions. Correspondingly, only model grid columns with nonzero surface rainfall are considered in the analysis. We also limit the comparison of IWC to those levels in the vertical with temperatures less than −5°C to minimize brightband effects on the radar-retrieved IWC.

The comparison focuses on a west–east cross section box from the Willamette River valley to the Cascade crest (dashed box in Fig. 1) within the 1.33-km domain and RTX radar range to assess the orographic precipitation enhancement. The box is chosen to minimize the influence of the radar's cone of silence and excludes regions with severe radar beam blocking. The terrain within the box gradually increases in height toward the east.

### c. *Storm selection and categorization*

In this study, a heavy precipitation event is defined as a day on which either observed or model mean rain gauge precipitation within the 1.33-km domain is over 12.7 mm (0.5 in.) over a 24-h period starting at 0000 UTC. This threshold was chosen to focus on larger, longer-lasting storms. From the resultant 90 events, we first removed the poorly simulated events (5 days) based on a comparison of the SLE sounding at 1.5 km MSL (near the crest level of Cascades) with the model. More specifically, those

TABLE 1. A summary of storm days [77 total, either observed or model daily-mean precipitation larger than 0.5 in. (~1.3 cm); refer to text for more details]. Warm storms are defined as those with temperature at 1.5 km MSL greater than −1°C, and cold storms are those with temperature at 1.5 km MSL less than −1°C. The number pair denotes days (mean precipitation bias score); Fqv denotes the integrated moisture flux. Precipitation bias scores significantly different from zero at the 99% level using a one-tailed *t* test also have the 99% confidence interval denoted.

| Total storms (77) | Warm storms (46) | Cold storms (31) |
|---|---|---|
| Fqv over | 12 (1.74 ± 0.52) | 5 (1.42) |
| Fqv good | 33 (1.15 ± 0.15) | 23 (1.48 ± 0.18) |
| Fqv under | 1 (1.01) | 3 (1.17) |

storms with an absolute temperature error greater than 4 K or wind direction error greater than 25° azimuth at 1.5 km MSL were removed from the study dataset. A failure to reproduce these basic conditions in the model is likely related to a poor initialization. We further restricted the analysis to 77 days with predicted or observed southwesterly (180°–270°) winds at 1.5 km MSL, so that the radiosonde at Salem is reasonably representative of the inflow air going over the Cascades in our comparison box. Freezing-level height relative to the mountain heights determines precipitation types (rain or snow) and fallout (rain falls much faster than snow). The average Cascades crest in the 1.33-km model domain is about 1.6 km MSL; thus, these storms were partitioned into warm or cold storms based on the freezing-level height above or below Cascades crest. Specifically, warm (cold) storms are those storms having SLE temperatures at 1.5 km MSL greater (less) than −1°C. Consequently, the dominant precipitation type over the model domain is rain and snow for warm and cold storms, respectively. We also categorized storms based on the model-integrated moisture flux relative bias (>0.2, ''overprediction''; <−0.2, ''underprediction''; and ''good'' or ''well predicted'' otherwise) in Table 1. Finally, to separate the effects of errors in upwind moisture flux and other synoptic forcing from errors in mesoscale processes and model physics, we focused on 38 well-simulated storms, which have relative biases of wind speed at 1.5 km MSL and integrated moisture flux less than 0.2 and have a temperature bias at 1.5 km MSL less than 1 K (Table 2). There are 16 cold storms and 22 warm storms among the 38 well-simulated storms (Table 2).

TABLE 2. A summary of well-predicted storm days (38 in total; refer to days with the relative absolute bias of wind speed and integrated moisture flux less than 0.2 and the absolute bias of temperature less than 1 K). Numbers significantly different from zero at the 99% level using a one-tailed *t* test also have the 99% confidence interval denoted.

| Well-predicted storms (38) | Precipitation bias score | Model DR | Observed DR |
|---|---|---|---|
| Cold storms (16) | 1.57 ± 0.21 | 0.31 ± 0.08 | 0.19 ± 0.03 |
| Warm storms (22) | 1.16 ± 0.17 | 0.19 ± 0.02 | 0.17 ± 0.09 |

## 3. Results

### *a. Seasonal precipitation, kinematics, and thermodynamics evaluation*

The heaviest precipitation accumulations within the 1.33-km domain (500–700 cm), based on the sum of two cool seasons, are situated over some of the narrow ridges that are exposed to southerly or southwesterly low-level flow as well as the isolated volcanic peaks (Fig. 2a). Observations also show large precipitation values (200–400 cm) over other ridges and near high mountain peaks. For example, precipitation up to 697 cm was recorded near Mount Rainer. Small-scale variations of model precipitation are hard to evaluate using the sparse precipitation gauges over the area. Minder et al. (2008) found persistent precipitation variation over approximately 10-km-wide ridges and valleys in the western Olympic Mountains, Washington, in both observations and MM5 simulations. This indicates some of the small-scale variation of model precipitation may be real. Precipitation minima (180–330 cm) are located within the Cascade valleys and the lee of high volcanic peaks. There are also two widespread precipitation minima in the lowland areas of the Columbia River (150–240 cm) and the lee of the Cascades (30–90 cm). The 1.33-km MM5 simulated the seasonal precipitation within 30% of observed precipitation at many of the precipitation gauge sites (orange diamonds in Fig. 2b). Precipitation overprediction (bias > 130%) is preferentially occurring just upstream (southwest) of the Cascade foothills and in the immediate lee of Cascades. This indicates MM5 simulations might have some mesoscale dynamical biases, such as the mountain wave and associated ascent shifted too far upstream aloft and not enough subsidence in the lee. However, because of the poor resolution of the radial velocity data over the Cascades from the KRTX radar over the mountain area, we are not able to detect a clear signal.

The average wind speed, wind direction, moisture, and moisture flux profiles of all 77 storms are shown in Fig. 3. The MM5 overestimates the winds at SLE by 1–1.5 m $s^{-1}$ in a layer between 0.5 and 1 km MSL, whereas it underpredicts the flow by about 2 m $s^{-1}$ above 2.5 km MSL. This overestimated wind in the boundary layer has been noted by Garvert et al. (2007) and Hahn and Mass (2009) in their simulations of orographic precipitation storms over the same region. The MM5 wind direction is generally 10° more subgeostrophic than observed above 2.5 km MSL,

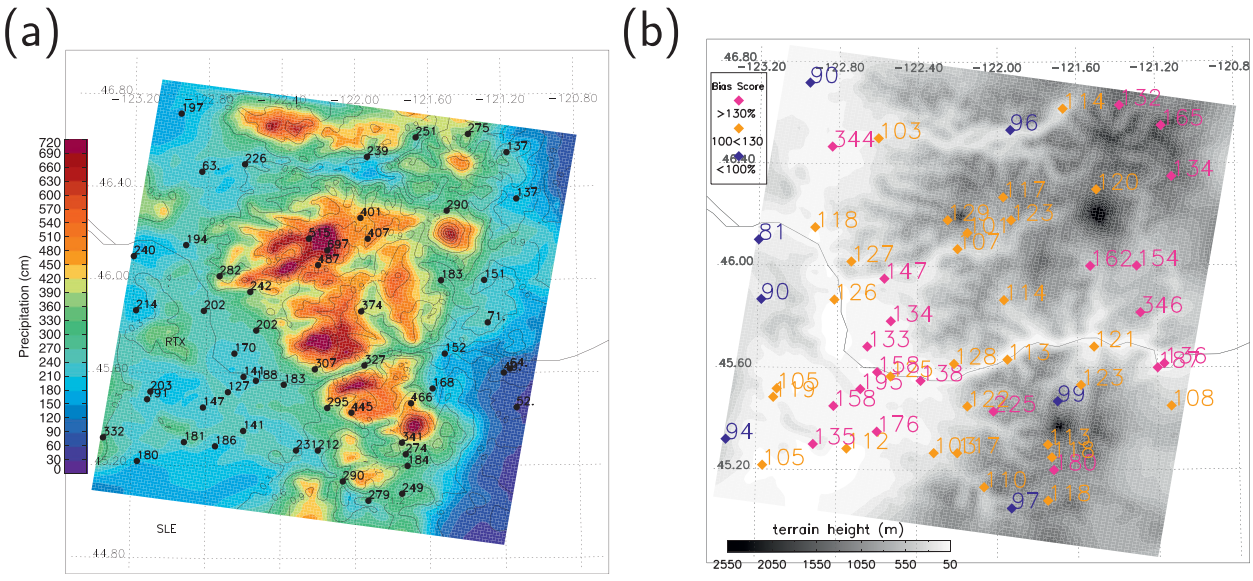


FIG. 2. (a) MM5 two-season total precipitation (color shaded, cm) for the 1.33-km model domain. Contour lines are terrain heights (km). The numbers denote the observed two-seasonal total precipitation (cm). (b) Model seasonal precipitation bias score (%).

but these biases are generally within the sampling uncertainty and not significant (not shown). The combination of overestimated moisture (~8%) below 1.2 km MSL and the overpredicted winds at low levels yields a mean moisture flux error of about 20 g $m^{-2}$ $s^{-1}$ (~25%) around 0.8 km MSL. This average moisture error (~8%) is larger than that at the model initialization time (~2%, not shown) and suggests that the moisture error is either advected from over the Pacific Ocean or developed during the model integration. The identification of sources for this moisture bias warrants further investigation in another study.

### b. *Impact of freezing level on model precipitation bias*

The integrated moisture fluxes at SLE and downstream orographic precipitation for the set of 77 storms are positively correlated, both within the MM5 ($r^2 = 0.75$) and the observations ($r^2 = 0.80$) (Fig. 4a). The subdivision

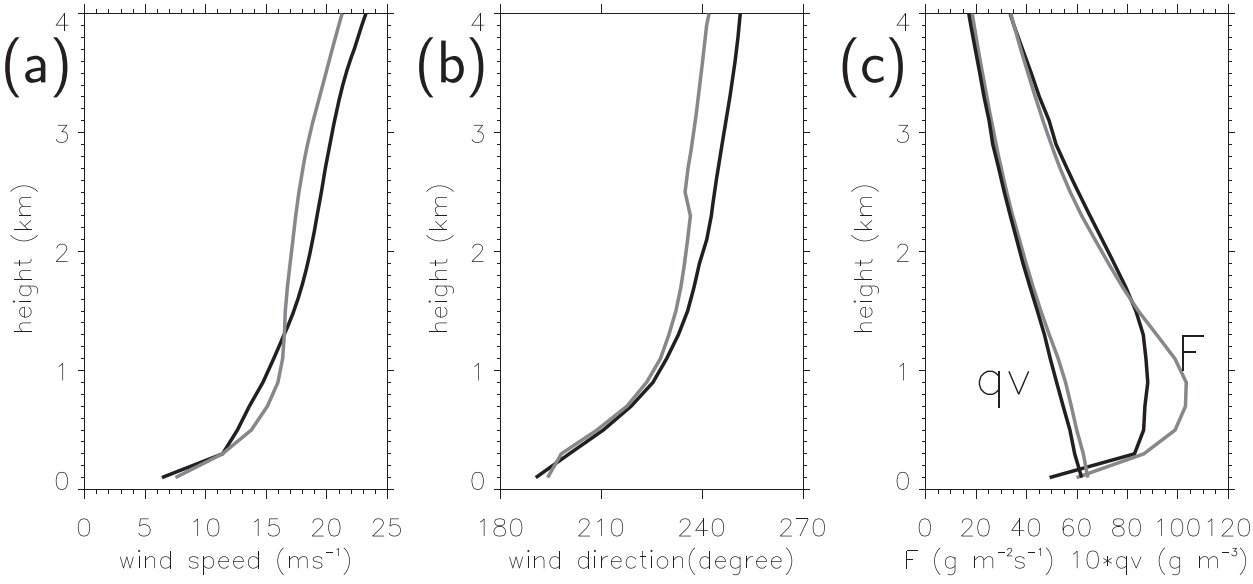


FIG. 3. (a) Total storms (77) averaged observed (black) and model (gray) wind speed profile. (b) As in (a), but for the wind direction. (c) As in (a), but for the moisture (qv) and moisture flux ($F$).

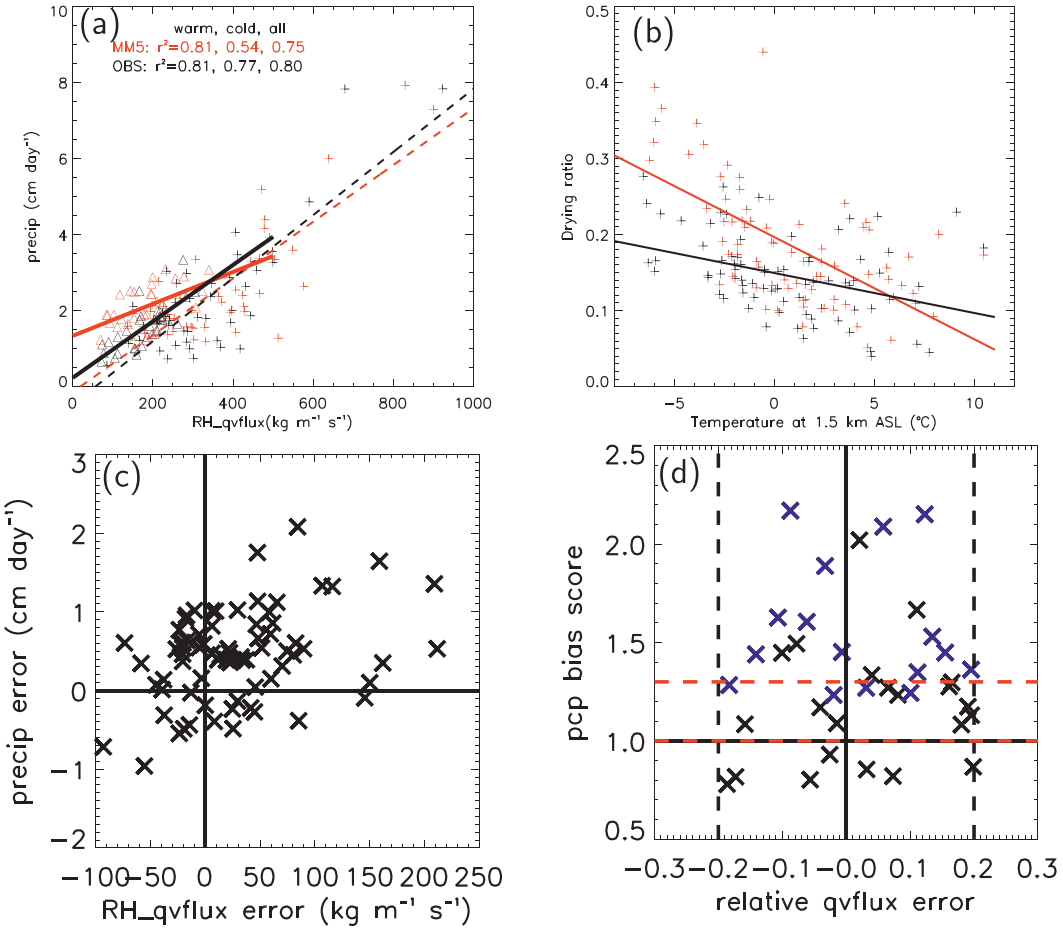


FIG. 4. (a) The correlation between the integrated RH-weighted moisture flux and precipitation for model (red) and observed (black). Crosses are warm days and triangles are cold days. Solid (dashed) lines are the linear fit for cold (warm) days. Correlation coefficients for warm, cold, and all storms are also labeled for MM5 and observation. These correlations are significantly different from zero at the 99% level using a one-tailed Student's *t* test. (b) Drying ratios change with temperatures at 1.5 km MSL for model (red) and observation (black). Solid lines are linear fits to the data. (c) Scatterplot between precipitation bias and the integrated moisture flux bias. (d) Scatterplot of model precipitation bias scores and the model relative integrated moisture flux bias for the 38 well-predicted days. Black crosses are warm days and blue crosses are cold days. The 1.0- and 1.3-bias-score lines are shown as two red dashed lines.

of the 77 storms into warm and cold subsets yields a slight improvement in the correlation for the warm storms ($r^2 = 0.81$ for both MM5 and observed) and a decrease in correlation for cold storms (MM5 $r^2 = 0.54$, observed $r^2 = 0.77$). All of these correlations are significant at the 99% level using a one-tailed Student's *t* test. Unlike warm storms, there is a large difference in the magnitude of correlation between moisture flux and precipitation in the MM5 versus observed for cold storms. This discrepancy between model and observations is a clue that some kind of model bias is occurring in the cold storms more frequently than the warm storms.

An alternate way of describing the relationship between inflow moisture flux and precipitation is in terms of drying ratio (Smith et al. 2005). Drying ratio is defined here as the ratio of the precipitation fallout over the 1.33-km domain divided by the water vapor flux approaching the barrier. Precipitation fallout uses the mean precipitation at 56 gauge stations in the domain for both observations and model. The model domain-mean precipitation is generally well represented by the precipitation at 56 gauge stations, though there are variations from storm to storm (not shown). Note that water vapor flux is not weighted by RH so that our DR calculation will be directly comparable with other calculations made using the Smith et al. (2005) definition. In general, drying ratio increases with decreasing temperatures at 1.5 km MSL (Fig. 4b). This finding is

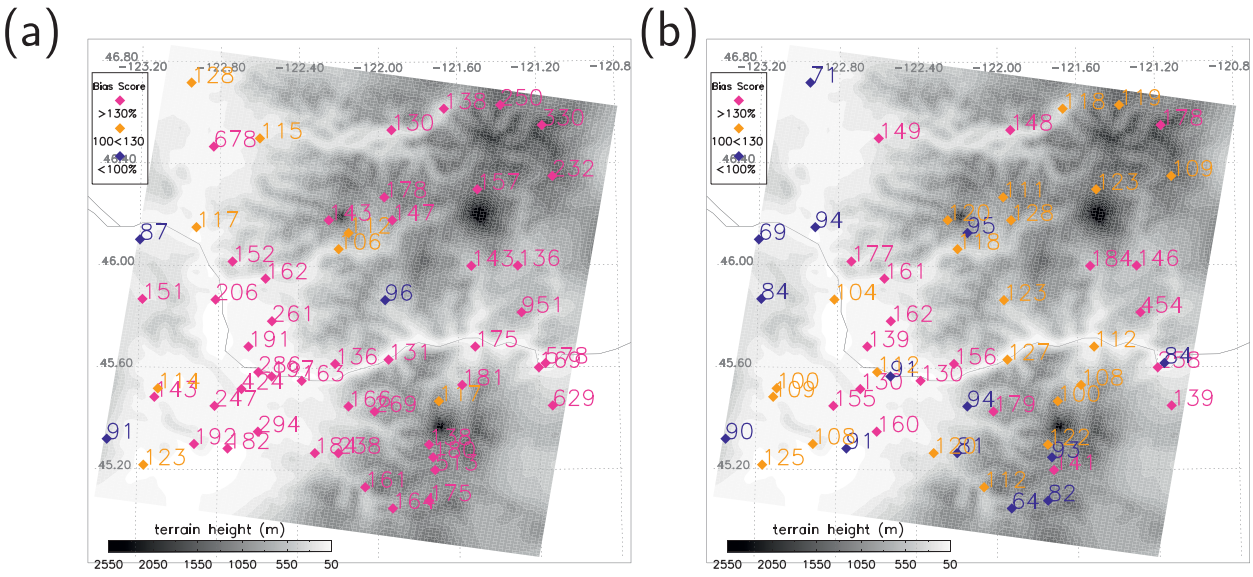


FIG. 5. (a) Model-mean precipitation bias scores for the cold well-predicted storms (16 days). (b) As in (a), but for the warm well-predicted storms (22 days).

consistent with Krishbaum and Smith's (2008) results and reflects increased precipitation efficiency with decreasing temperature. Examination of the scatter in Fig. 4b indicates a tendency for the model to overpredict drying ratio compared to observations, particularly for cold storms. The cold storm drying ratio overestimates of about 30%–50% in the model indicate that too much water vapor is being removed as precipitation by the model BMP. The average drying ratio for cold storms is 0.31 for MM5 and 0.19 for observed (Table 2). Considering the high correlation between moisture flux and precipitation for model and observations (Fig. 4a), it is expected that the moisture flux error is also highly related to the precipitation error. This is generally the case (Fig. 4c), but some storms have moisture flux and precipitation errors of different signs. This suggests that there are other factors influencing model precipitation error besides moisture flux error. Among the 38 well-simulated forecasts, MM5 always overestimates precipitation for cold storms with 12 days falling into our overprediction category with bias scores greater than 1.3 and 4 days with bias scores near 1.2 (blue crosses in Fig. 4d). This overprediction tendency for cold storms seems to be larger than what can be accounted for by the lack of use of a PDA scheme and larger gauge undercatchment error for cold storms.

The spatial distribution of precipitation biases (Fig. 5) also provides supporting evidence that the overprediction bias for cold storms is systematic across the model domain. The mean precipitation bias scores at gauge locations for cold storms show that the 1.33-km MM5 overpredicts precipitation by more than 50% over a large area of the domain including valley, windward-slope, and mountain-lee locations (Fig. 5a) resulting in an average bias score of 1.57 (Table 2). Overprediction at rain-only regions for cold storms (lowland in Fig. 5a) indicates such bias is not just related to the increased undercatchment for snow. Overprediction over such a wide range of topography suggests some kind of systematic error in model microphysics. Warm storms, in contrast, show a spatial pattern of biases with a more even mix of overpredicted, underpredicted, and well-predicted gauge locations (Fig. 5b), resulting in an average bias score of 1.16 (Table 2).

### c. *Comparisons with radar*

To relate the surface precipitation biases with cloud and precipitation aloft, we compared model IWC with radar-retrieved IWC and model-derived reflectivity with observed reflectivity. The comparisons are done over the west–east box (dashed box Fig. 1) between SLE and Portland and extend from the Willamette Valley to the windward slopes of Cascades. Figures 6a,c show the average reflectivity and IWC cross sections from the MM5 and the radar for the well-predicted cold and warm storms (Table 2). To weight each day equally, daily-mean reflectivities and IWC are computed first and then averaged for the final average.

For both warm and cold storms, the observed radar reflectivity and IWC contours (Figs. 6a,b) slope up approaching the Cascades, indicating a prominent orographic precipitation enhancement. In contrast, such

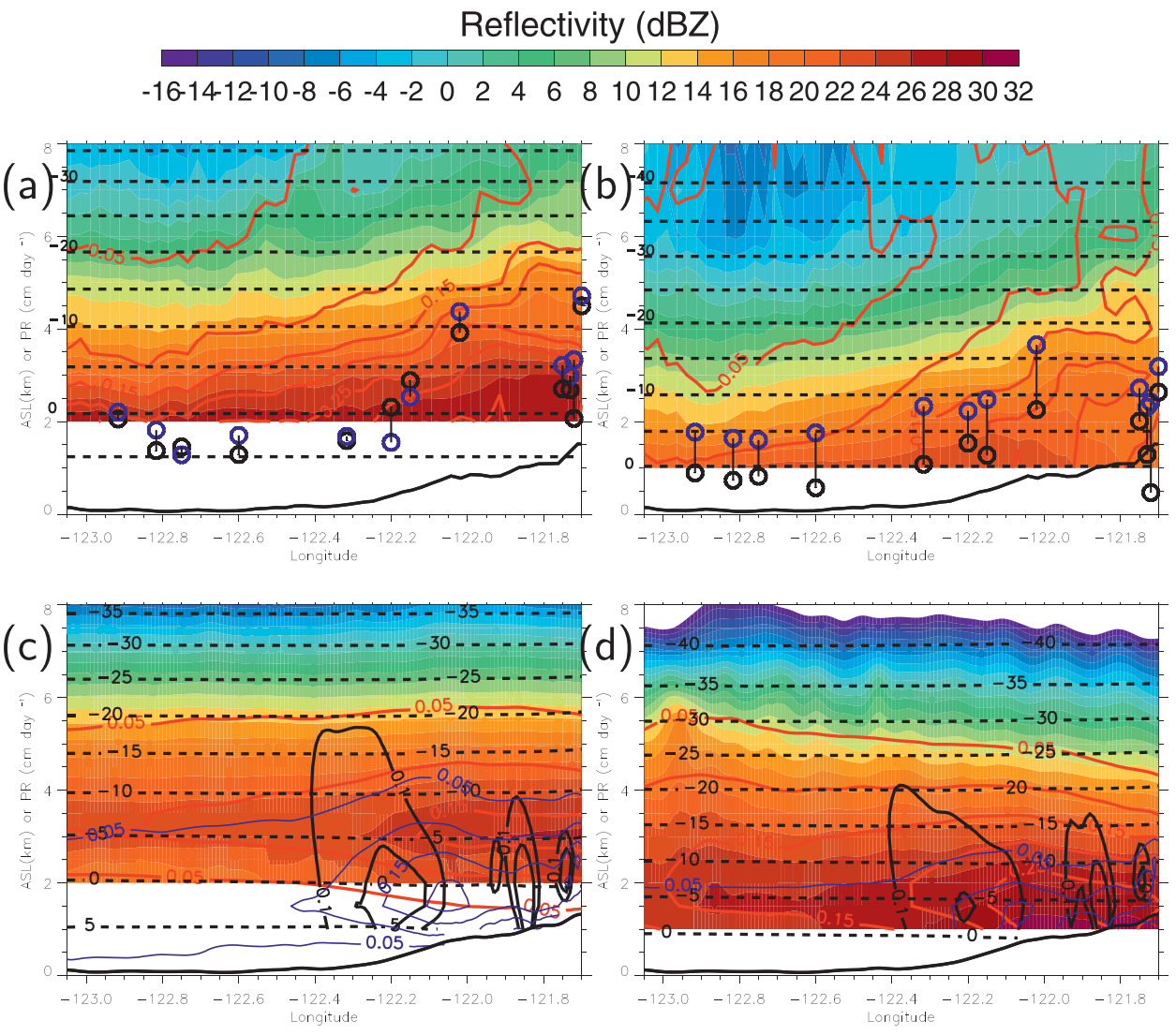


FIG. 6. Mean radar reflectivities (dB$Z$) in the thin black dashed west–east box in Fig. 1 for (a) the 22 warm storms and (b) the 16 cold storms. Red contours are radar-retrieved IWC. Blue and black circles are model and observed mean precipitation at stations in the west–east box. Black dashed lines are temperatures from the SLE sounding. (c) As in (a), but for the model-derived reflectivities (color shaded) of warm storms with IWC (red solid lines, interval is 0.05 g m$^{-3}$), vertical motion (black solid lines), liquid water content (blue lines, interval is 0.05 g m$^{-3}$), and temperatures (black dashed lines). (d) As in (c), but for model cold storms. The black thick line denotes the terrain heights. Reflectivities are blank for temperatures above 0°C for the model and radar.

sloping is not present in the model output (Figs. 6c,d). In addition, the relative differences between reflectivities (and IWC) in warm storms versus cold storms differ in the observations versus the model. The observed radar reflectivities are several decibels higher within the same temperature zone in the warm storms as compared to the cold storms. Consistently, the radar-retrieved IWC of the warm storms is about 50% larger than that of the cold storms. In contrast, both model-derived reflectivity and IWC are larger for the cold storms. For example, the contours of the MM5 IWC field for the cold storms (Fig. 6d) show a large region of values greater than 0.15 g m$^{-3}$ extending from the Cascades westward across the domain. In comparison, IWC $>$ 0.15 g m$^{-3}$ for warm storms is present only over the Cascades in a layer near −6°C. This difference in the spatial distribution of IWC translates into model-estimated reflectivity values for the cold storms (Fig. 6d) of 20–30 dB$Z$ within the −15° to 0°C layer, which are about 5 dB$Z$ larger than the estimated reflectivities for the warm storms in the same temperature zone (Fig. 6c). The high values of model IWC and derived reflectivity

aloft for cold storms yield a surface precipitation overprediction for cold storms. For example, MM5 overpredicts by 100%–200% at most gauge stations within the west–east box for cold storms (blue and black circles in Fig. 6b). Gauge undercatchment can be larger for cold storms than warm storms and increases the overprediction bias for the cold storms. Surface precipitation is better predicted for warm storms (Fig. 6a) indicating that the model's IWC values in warm storms are more realistic.

We interpret that overprediction errors tend to occur more frequently or dominate in the modeled cold storms based on relative differences in IWC and reflectivity values for cold versus warm storms. Modeled cold storms have higher IWC and reflectivity values than modeled warm storms. This relative relationship is the reverse of the observed higher values of IWC and reflectivity in warm storms compared to that in cold storms.

What are the reasons for the persistent and widespread overprediction bias for cold storms? With an overall well-predicted synoptic forcing and moisture flux, such bias can still be generated by mesoscale processes and model physics, especially the BMP. For example, the too-deep echoes over the Willamette Valley for modeled cold storms (Fig. 6d) might suggest some mountain wave forcing and convective instability issues. We propose a plausible explanation focusing on cloud and precipitation processes. Snow depositional and riming processes are the two primary ice phase growth mechanisms for winter orographic precipitation. The snow depositional growth parameterization in BMPs has large uncertainties associated with particle capacitance, particle size distribution, and particle mass and fall velocity characteristics. For example, Lin and Colle (2009) found snow aloft in the depositional growth zone for an orographic storm was reduced by 60% when the capacitance for aggregates instead of spheres was used.

Most BMPs include snow and graupel, but partially rimed particles in mixed-phase orographic precipitation systems (e.g., Rauber 1992; Woods et al. 2008) are not well represented. This could potentially underestimate graupel and its associated fallout in the BMP. The riming process not only impacts the precipitation efficiency but also modifies the precipitation fallout due to the substantially different fall speeds of snow and graupel particles. Consequently, the supercooled water production and the resultant riming process need to be better represented in BMPs.

Some potential causes for the different model simulation of hydrometeors aloft and surface precipitation for warm and cold storms are explored. For both warm and cold storms, MM5 has maximum vertical motion near 2 km MSL over the windward slopes of the Cascades (Figs. 6c,d). For the cold storms (mean freezing level near 1 km MSL), three associated factors combine to produce large values of snow (up to 0.25 g $m^{-3}$) above the windward slopes at 2-km altitude. First, temperatures (of about −10°C) within the ascent region for cold storms (Fig. 6d) favor snow depositional growth (Rogers and Yau 1989). Second, a snow depositional growth parameterization with a positive bias tends to induce snow overprediction aloft (Lin and Colle 2009). Last, there is a positive feedback cycle as larger snow values further enhance snow depositional growth since snow depositional growth increases with snow amount. In contrast, for the warm storms (mean freezing level near 2 km MSL; Fig. 6c), the maximum upward motion is at temperatures near 0°C. This increases cloud liquid water generation and favors riming growth and graupel production. Cloud water is as high as 0.2 g $m^{-3}$ in the ascent regions of the warm storms. The larger fall speed of graupel compared to snow results in more efficient IWC fallout where riming is active. As a result, less IWC remains aloft where abundant supercooled cloud water exists. Overall, an overestimated snow depositional growth has a larger impact on cold storms than on warm storms because of the larger contribution of snow depositional growth to the total surface precipitation for cold storms.

Snow overprediction aloft has been noted in several orographic precipitation case studies using different BMPs (Garvert et al. 2005b; Lin and Colle 2009; Milbrandt et al. 2010). The results from this study suggest that the overestimated IWC aloft for cold storms is occurring over many events, and it is likely from some systematic bias associated with ice microphysical processes, such as snow depositional growth, within the BMP.

## 4. Discussion and summary

Two cool seasons of high-resolution MM5 simulations over the Pacific Northwest were evaluated using precipitation gauge data, an upstream sounding, and an NWS WSR-88D. The model could realistically simulate the seasonal precipitation generally within 90%–130% of the observed values over most of the rain gauge sites (Fig. 2b). In concurrence with previous studies, for the seasonal set of 77 storms, there is a high correlation between moisture flux and surface precipitation in both the observed ($r^2 = 0.80$) and modeled storms ($r^2 = 0.75$). As a result, model precipitation error typically increases with increasing moisture flux error.

The 77 storm days were partitioned into warm storm (freezing level above the Cascades crest) and cold storm (freezing level below the Cascades crest) categories. Drying ratios were about 30%–50% higher for the

model compared to observations for the cold storms. These systematically higher drying ratios for MM5 indicate that too much water vapor is being removed as precipitation in the cold storms. The simulated precipitation for the cold storms was less correlated with the moisture flux ($r^2 = 0.54$) than was the observed ($r^2 = 0.77$), which is likely a consequence of the surface precipitation overprediction in the model for the cold storms. In contrast, both the model and observed values had a good correlation between precipitation and moisture flux for the warm storms ($r^2 = 0.81$), and there was less widespread precipitation overprediction in the model for warm storms.

The well-simulated subset of storms (38 cases), those with errors less than 20% in wind speed and moisture flux and a temperature bias less than 1 K, were also separated into warm and cold storm categories in order to better understand the underlying physics. Unlike the 22 well-simulated warm storms, the 16 well-simulated cold storms overestimated precipitation at gauge locations across the Willamette Valley and the windward and lee slopes of the Cascades within the model domain. Consistent with surface precipitation overprediction for the cold storms, MM5 has larger reflectivity and IWC aloft than the observed radar reflectivity and retrieved IWC. In contrast, for warm storms, MM5 has better agreement with the radar in terms of both reflectivity and IWC, which translates into a better prediction of surface precipitation. Observed radar reflectivity and IWC is larger for the warm storms than for the cold storms, but model reflectivity and IWC is larger for the cold storms than for the warm storms. One possible reason for the persistent overprediction of surface precipitation and IWC aloft for the cold storms might be related to a potential positive bias of the snow depositional growth formulation in the BMP. An additional amplification to the overprediction of IWC aloft within the modeled cold storms is the juxtaposition of the upward motion associated with the mountain wave and air temperatures favorable for snow depositional growth. Other mesoscale processes, such as convective cells and shear, may also contribute to the noted model bias and warrant further investigation. This analysis also highlights the benefit of using three-dimensional data from an operational radar in addition to surface gauge measurements for model precipitation evaluation over mountainous terrain.

There have been several recent efforts to improve BMPs for mesoscale models (e.g., Woods et al. 2007; Morrison and Grabowski 2008, 2010; Dudhia et al. 2008; Lin and Colle 2011). The abrupt transition from snow to graupel in some BMPs neglects the abundance of partially rimed particles in mixed-phase clouds. Lin and Colle (2011) proposed a new BMP that includes a gradual change from snow to graupel and thus represents the partially rimed particles. A reduced snow depositional growth rate appropriate for aggregates and inclusion of partially rimed particles might help improve the noted systematic overprediction bias for the cold storms. Future work will involve using WRF with some other BMPs in this region to determine generality of our results.

Large samples of storms help the detection of relatively robust model precipitation biases. This study is a preliminary effort toward this direction. Nevertheless, precipitation simulation involves various interacting dynamical and physical processes, and it is a challenge to identify and quantify the sources of precipitation bias. Focusing on certain types of storms enables us to narrow down the possible paths contributing to precipitation bias. Future work includes utilizing other available observations, such as integrated water vapor from a global positioning system (GPS), to better quantify the model moisture bias development.

*Acknowledgments.* Special thanks to David Stark and Jake Crouch for their assistance in radar data processing. This research was supported by the Office of Science (Biological and Environmental Research), U.S. Department of Energy (Lin), and the National Science Foundation Grants ATM-0908288 (Colle) and ATM-0908420 (Yuter). Comments from three anonymous reviewers significantly improved the manuscript. Any opinions, findings, and conclusions or recommendations expressed in this material are those of the authors and do not necessarily reflect the views of the National Science Foundation.

## REFERENCES

Colle, B. A., and C. F. Mass, 2000: The 5–9 February 1996 flooding event over the Pacific Northwest: Sensitivity studies and evaluation of the MM5 precipitation forecasts. *Mon. Wea. Rev.,* **128,** 593–617.

——, K. J. Westrick, and C. F. Mass, 1999: Evaluation of MM5 and Eta-10 precipitation forecasts over the Pacific Northwest during the cool season. *Wea. Forecasting,* **14,** 137–154.

——, M. F. Garvert, J. B. Wolfe, C. F. Mass, and C. P. Woods, 2005: The 13–14 December 2001 IMPROVE-2 event. Part III: Simulated microphysical budgets and sensitivity studies. *J. Atmos. Sci.,* **62,** 3535–3558.

——, Y. Lin, S. Medina, and B. Smull, 2008: Orographic modification of convection and flow kinematics by the Oregon coastal range and Cascades during IMPROVE-2. *Mon. Wea. Rev.,* **136,** 3894–3916.

Cressman, G., 1959: An operational objective analysis system. *Mon. Wea. Rev.,* **87,** 367–374.

Dudhia, J., 1989: Numerical study of convection observed during the winter monsoon experiment using a mesoscale two-dimensional model. *J. Atmos. Sci.,* **46,** 3077–3107.

——, H. Song-You, and K. Lim, 2008: A new method for representing mixed-phase particle fall speeds in bulk microphysics parameterizations. *J. Meteor. Soc. Japan,* **86A,** 33–44.

Falvey, M., and R. Garreaud, 2007: Wintertime precipitation episodes in central Chile: Associated meteorological conditions and orographic influences. *J. Hydrometeor.,* **8,** 171–193.

Garvert, M. F., B. A. Colle, and C. F. Mass, 2005a: The 13–14 December 2001 IMPROVE-2 event. Part I: Synoptic and mesoscale evolution and comparison with a mesoscale model simulation. *J. Atmos. Sci.,* **62,** 3474–3492.

——, C. P. Woods, B. A. Colle, C. F. Mass, P. V. Hobbs, M. T. Stoelinga, and J. B. Wolfe, 2005b: The 13–14 December 2001 IMPROVE-2 event. Part II: Comparisons of MM5 model simulations of clouds and precipitation with observations. *J. Atmos. Sci.,* **62,** 3520–3534.

——, B. Smull, and C. Mass, 2007: Multiscale mountain waves influencing a major orographic precipitation event. *J. Atmos. Sci.,* **64,** 711–737.

Groisman, P. Ya., and D. R. Legates, 1994: The accuracy of United States precipitation data. *Bull. Amer. Meteor. Soc.,* **75,** 215–227.

Grubisić, V., R. K. Vellore, and A. W. Huggins, 2005: Quantitative precipitation forecasting of wintertime storms in the Sierra Nevada: Sensitivity to the microphysical parameterization and horizontal resolution. *Mon. Wea. Rev.,* **133,** 2834–2859.

Hahn, R., and C. Mass, 2009: The impact of positive-definite moisture advection and low-level moisture flux bias over orography. *Mon. Wea. Rev.,* **137,** 3055–3071.

Heymsfield, A. J., and Coauthors, 2008: Testing IWC retrieval methods using radar and ancillary measurements with in situ data. *J. Appl. Meteor. Climatol.,* **47,** 135–163.

Hogan, R. J., M. P. Mittermaier, and A. J. Illingworth, 2006: The retrieval of ice water content from radar reflectivity factor and temperature and its use in evaluating a mesoscale model. *J. Appl. Meteor. Climatol.,* **45,** 301–317.

James, P., A. Stohl, N. Spichtinger, S. Eckhardt, and C. Forster, 2004: Climatological aspects of the extreme European rainfall of August 2002 and a trajectory method for estimating the associated evaporative source regions. *Nat. Hazards Earth Syst. Sci.,* **4,** 733–746.

Janjić, Z. I., 1994: The step-mountain eta coordinate model: Further developments of the convection, viscous sublayer, and turbulence closure schemes. *Mon. Wea. Rev.,* **122,** 927–945.

Kain, J. S., 2004: The Kain–Fritsch convective parameterization: An update. *J. Appl. Meteor.,* **43,** 170–181.

——, and J. M. Fritsch, 1993: Convective parameterization for mesoscale models: The Kain–Fritsch scheme. *The Representation of Cumulus Convection in Numerical Models, Meteor. Monogr.,* No. 24, Amer. Meteor. Soc., 165–170.

Kirshbaum, D. J., and R. B. Smith, 2008: Temperature and moist-stability effects on midlatitude orographic precipitation. *Quart. J. Roy. Meteor. Soc.,* **134,** 1183–1199.

Leung, L. R., and Y. Qian, 2003: The sensitivity of precipitation and snowpack simulations to model resolution via nesting in regions of complex terrain. *J. Hydrometeor.,* **4,** 1025–1043.

Lin, Y., and B. A. Colle, 2009: The 4–5 December 2001 IMPROVE-2 Event: Observed microphysics and comparisons with the Weather Research and Forecasting model. *Mon. Wea. Rev.,* **137,** 1372–1392.

——, and ——, 2011: A new bulk microphysical scheme that includes riming intensity and temperature-dependent ice characteristics. *Mon. Wea. Rev.,* **139,** 1013–1035.

Mass, C. F., D. Ovens, K. Westrick, and B. A. Colle, 2002: Does increasing horizontal resolution produce more skillful forecasts? *Bull. Amer. Meteor. Soc.,* **83,** 407–430.

Milbrandt, J. A., M. K. Yau, J. Mailhot, and S. Bélair, 2008: Simulation of an orographic precipitation event during IMPROVE-2. Part I: Evaluation of the control run using a triple-moment bulk microphysics scheme. *Mon. Wea. Rev.,* **136,** 3873–3893.

——, ——, ——, ——, and R. McTaggart-Cowan, 2010: Simulation of an orographic precipitation event during IMPROVE-2. Part II: Sensitivity to the number of moments in the bulk microphysics scheme. *Mon. Wea. Rev.,* **138,** 625–642.

Minder, J. R., D. R. Durran, G. H. Roe, and A. M. Anders, 2008: The climatology of small-scale orographic precipitation over the Olympic Mountains: Patterns and processes. *Quart. J. Roy. Meteor. Soc.,* **134,** 817–839.

Morrison, H., and W. W. Grabowski, 2008: A novel approach for representing ice microphysics in models: Description and tests using a kinematic framework. *J. Atmos. Sci.,* **65,** 1528–1548.

——, and ——, 2010: An improved representation of rimed snow and conversion to graupel in a multicomponent bin microphysics scheme. *J. Atmos. Sci.,* **67,** 1337–1360.

Muller, M., and M. Kaspar, 2011: Association between anomalies of moisture flux and extreme runoff events in the south-eastern Alps. *Nat. Hazards Earth Syst. Sci.,* **11,** 915–920.

Neiman, P. J., F. M. Ralph, A. B. White, D. E. Kingsmill, and P. O. G.Persson, 2002: The statistical relationship between upslope flow and rainfall in California's coastal mountains: Observations during CALJET. *Mon. Wea. Rev.,* **130,** 1468–1492.

——, L. J. Schick, F. M. Ralph, M. Hughes, and G. A. Wick, 2011: Flooding in western Washington: The connection to atmospheric rivers. *J. Hydrometeor.,* **12,** 1337–1358.

Protat, A., J. Delanoë, D. Bouniol, A. J. Heymsfield, A. Bansemer, and P. Brown, 2007: Evaluation of ice water content retrievals from cloud radar reflectivity and temperature using a large airborne in situ microphysical database. *J. Appl. Meteor. Climatol.,* **46,** 557–572.

Ralph, F. M., and Coauthors, 2005: Improving short-term (0–48 h) cool-season quantitative precipitation forecasting: Recommendations from a USWRP workshop. *Bull. Amer. Meteor. Soc.,* **86,** 1619–1632.

Rauber, R. M., 1992: Microphysical structure and evolution of a central Sierra Nevada orographic cloud system. *J. Appl. Meteor.,* **31,** 3–24.

Richard, E., A. Buzzi, and G. Zängl, 2007: Quantitative precipitation forecasting in the Alps: The advances achieved by the Mesoscale Alpine Programme. *Quart. J. Roy. Meteor. Soc.,* **133,** 831–846.

Roebber, P. J., K. L. Swanson, and J. K. Ghorai, 2008: Synoptic control of mesoscale precipitating systems in the Pacific Northwest. *Mon. Wea. Rev.,* **136,** 3465–3476.

Rogers, R. R., and M. K. Yau, 1989: *A Short Course in Cloud Physics.* Pergamon Press, 293 pp.

Schlemmer, L., O. Martius, M. Sprenger, C. Schwierz, and A. Twitchett, 2010: Disentangling the forcing mechanisms of a heavy precipitation event along the Alpine south side using potential vorticity inversion. *Mon. Wea. Rev.,* **138,** 2336–2353.

Skamarock, W. C., 2006: Positive-definite and monotonic limiters for unrestricted-time-step transport schemes. *Mon. Wea. Rev.,* **134,** 2241–2250.

——, and Coauthors, 2008: A description of the advanced research WRF version 3. NCAR Tech. Note NCAR/TN-475+STR, 113 pp. [Available online at http://www.mmm.ucar.edu/wrf/users/docs/arw_v3_bw.pdf.]

Smith, B. L., S. E. Yuter, P. J. Neiman, and D. E. Kingsmill, 2010: Water vapor fluxes and orographic precipitation over Northern California associated with a landfalling atmospheric river. *Mon. Wea. Rev.,* **138,** 74–100.

Smith, R. B., 1979: The influence of mountains on the atmosphere. *Advances in Geophysics,* Vol. 21, Academic Press, 87–230.

——, and J. P. Evans, 2007: Orographic precipitation and water vapor fractionation over the southern Andes. *J. Hydrometeor.,* **8,** 3–19.

——, Q. F. Jiang, M. G. Fearon, P. Tabary, M. Dorninger, J. D. Doyle, and R. Benoit, 2003: Orographic precipitation and air mass transformation: An alpine example. *Quart. J. Roy. Meteor. Soc.,* **129B,** 433–454.

——, I. Barstad, and L. Bonneau, 2005: Orographic precipitation and Oregon's climate transition. *J. Atmos. Sci.,* **62,** 177–191.

Stauffer, D. R., and N. L. Seaman, 1990: Use of four-dimensional data assimilation in a limited-area mesoscale model. Part I: Experiments with synoptic-scale data. *Mon. Wea. Rev.,* **118,** 1250–1277.

Theriault, J. M., R. Rasmussen, K. Ikeda, and S. Landolt, 2012: Dependence of snow gauge collection efficiency on snowflake characteristics. *J. Appl. Meteor. Climatol.,* **51,** 745–762.

Thompson, G., R. M. Rasmussen, and K. Manning, 2004: Explicit forecasts of winter precipitation using an improved bulk microphysics scheme. Part I: Description and sensitivity analysis. *Mon. Wea. Rev.,* **132,** 519–542.

——, P. R. Field, R. M. Rasmussen, and W. D. Hall, 2008: Explicit forecasts of winter precipitation using an improved bulk microphysics scheme. Part II: Implementation of a new snow parameterization. *Mon. Wea. Rev.,* **136,** 5095–5115.

Turner, D. D., B. M. Lesht, S. A. Clough, J. C. Liljegren, H. E. Revercomb, and D. C. Tobin, 2003: Dry bias and variability in Vaisala RS80-H radiosondes: The ARM experience. *J. Atmos. Oceanic Technol.,* **20,** 117–132.

Woods, C. P., M. T. Stoelinga, and J. D. Locatelli, 2007: The IMPROVE-1 storm of 1–2 February 2001. Part III: Sensitivity of a mesoscale model simulation to the representation of snow particle types and testing of a bulk microphysical scheme with snow habit prediction. *J. Atmos. Sci.,* **64,** 3927–3948.

——, ——, and ——, 2008: Size spectra of snow particles measured in wintertime precipitation in the Pacific Northwest. *J. Atmos. Sci.,* **65,** 189–205.

Yuter, S. E., D. A. Stark, J. A. Crouch, M. J. Payne, and B. A. Colle, 2011: The impact of varying environmental conditions on the spatial and temporal patterns of orographic precipitation over the Pacific Northwest near Portland, Oregon. *J. Hydrometeor.,* **12,** 329–351.